Available online at BCREC Website: https://bcrec.undip.ac.id

Bulletin of Chemical Reaction Engineering & Catalysis, 13 (2) 2018, 295-310

Research Article

Effects of Platinum and Palladium Metals on Ni/$Mg_{1-x}Zr_xO$ Catalysts in the CO_2 Reforming of Methane

Faris A. J. Al-Doghachi

Department of Chemistry, Faculty of Science, University of Basra, Basra, Iraq

Received: 25th October 2017; Revised: 2nd January 2018; Accepted: 18th January 2018; Available online: 11st June 2018; Published regularly: 1st August 2018

Abstract

Nickel, palladium, and platinum catalysts (1 wt.% each) supported on MgO and MgZrO to prepare Pt,Pd,Ni/$Mg_{1-x}Zr_xO$ catalysts (where x = 0, 0.03, 0.07, and 0.15), were synthesized by using co-precipitation method with K_2CO_3 as the precipitant. X-ray diffraction (XRD), X-ray fluorescence (XRF), X-ray photoelectron spectroscopy (XPS), Brunauer–Emmett–Teller (BET), transmission electron microscopy (TEM), H_2-temperature programmed reduction (H_2-TPR), and thermo gravimetric analysis (TGA) were employed to observe the characteristics of the prepared catalysts. The Pt,Pd,Ni/$Mg_{0.85}Zr_{0.15}O$ showed the best activity in dry reforming of methane (DRM) with 99 % and 91 % for CO_2 and CH_4 conversions, respectively and 1.28 for H_2/CO ratio at temperature 900 °C and 1:1 of CH_4:CO_2 ratio. The stability of Pt,Pd,Ni/$Mg_{0.85}Zr_{0.15}O$ catalyst in the presence and absence of low stream 1.25 % oxygen was investigated. Carbon formation and amount in spent catalysts were examined by TEM and TGA in the presence of stream oxygen. The results showed that the amount of carbon was suppressed and negligible coke formation (less than 3 %) was observed. Several effects were observed with ZrO_2 use as a promoter in the catalyst. Firstly, the magnesia cubic phase stabilized. Secondly, thermal stability and support for basicity increased. Thirdly, carbon deposition and the reducibility of Ni^{2+}, Pd^{2+}, and Pt^{2+} ions decreased.

Keywords: Biogas; Catalyst Deactivation; Dry Reforming; H_2 Production; Synthesis Gas

How to Cite: Al-Doghachi, F.A.J. (2018). Effects of Platinum and Palladium Metals on Ni/$Mg_{1-x}Zr_xO$ Catalysts in the CO_2 Reforming of Methane. *Bulletin of Chemical Reaction Engineering & Catalysis*, 13 (2): 295-310 (doi:10.9767/bcrec.13.2.1656.295-310)

Permalink/DOI: https://doi.org/10.9767/bcrec.13.2.1656.295-310

1. Introduction

Alternative energy resources are highly demanded because the reserves of fossil fuels are depleting very rapidly. Consequently, the use of greenhouse gases, such as CH_4 and CO_2, as an alternative energy source has gained more importance. The search for methane has ended with favorable results. Methane is readily available, and reserves that are bigger than crude oil reserves have been revealed. CH_4 can be obtained from shale gas and fermented wastes [1]. It is transformed into syngas (a mixture of CO and H_2), which can be produced through the use of steam, partial oxidation, or carbon dioxide in reforming reactions.

The dry-reforming process involves the conversion of CH_4 and CO_2, which are two of the cheapest and most abundant carbon-containing materials, into synthesis gas (Equation 1). This

* Corresponding Author.
E-mail: faris_jassim@yahoo.com
Telp: 009647800995900

reaction also has very important environmental implications because both methane and carbon dioxide are greenhouse gases, which may be converted into valuable product such as hydrogen. Further, due to its large heat of reaction and reversibility, this process has potential thermo-chemical heat-pipe applications for the recovery, storage, and transmission of solar and other renewable energy sources.

$$CH_4 + CO_2 \rightarrow 2CO + 2H_2 \quad \Delta H_{298}^{o} = 247.0 \text{ kJ/mol} \quad (1)$$

This synthesized gas has become an important raw material for fuels and/or for producing chemicals for industrial use. In fact, fossil fuel and biomass can undergo conversion into synthesis gas. However, for the purpose of industrial application of syngas, the H_2/CO molar ratios must be varied. For example, in the synthesis of methanol [2], the H_2/CO ratio required is 2. Meanwhile, under a single step process (H_2/CO ratio = 1), dimethyl ether can be synthesized [3,4]. It is worth noting that H_2/CO ratio plays a critical role in the process of producing syngas [5].

The reaction between DRM and noble metals, such as Pt, Rh, and Ru, is highly active [6]. Furthermore, these metals resist carbon from being formed more effectively compared with other transition metals [7], since Ni catalysts are more favorable with noble metals, such as Rh, Pt, Pd, or Ru. They increase the reaction of the catalysts, and they are more stable in their reaction against coke deposition when compared with that of the other non-favorable Ni catalysts [8]. For instance, bimetallic Ni-Pt that supports ZrO_2 shows that it is able to sustain a longer duration of activity time than monometallic Ni/ZrO_2. Thus, Ni-Pt catalyst has high potential for industrial application for DRM [9]. The activity and stability of trimetalic Pt-Pd-Ni catalysts are higher than those of the monometallic Ni catalyst [10]. These findings support the idea that Pt-Pd can be used in the prevention of the oxidation of Ni. In a research work on the use of favorable catalysts of Ni/MgO with Ce(III), the findings revealed more active catalytic activity and higher stability for Co-promoted catalysts. This result is supported by Ce-promoted catalysts, in which the resistance of coke deposition was high. As the catalytic activity of Ce-promoted catalysts increases because of their high affinity for oxygen species, the characteristics of the resistance of coke improve. Ce-promoted catalysts exhibited no favorable catalytic performance. The cause for the unfavorable catalytic activity in Ce-promoted catalyst is the segregation of Ce as CeO_2. This reaction occurred because of immiscibility with MgO that caused the increase of the size of Ni particles [11].

The present work describes the synthesis of Pt,Pd,Ni/$Mg_{1-x}Zr_xO$ catalysts (where x = 0, 0.03, 0.07, and 0.15) containing 1 % of each of Ni, Pd and Pt metals, in order to evaluate their activity, selectivity and stability, as well as their ability to decrease the deposition of carbon on the catalyst during the DRM reaction. The effect of 1.25 % O_2 on conversion of methane will be studied. The catalyst used in order to enhance the selectivity and stability in compare with to previous work [12].

2. Materials and Method

2.1 Preparation of catalysts

The co-precipitation method was used for the preparation of the catalysts, $Mg_{1-x}Zr_xO$ (x = 0.00, 0.03, 0.07, and 0.15). The support of MgO and promoter zirconia of ZrO_2 was prepared according to a literature method [12] by using a 0.1 M $ZrCl_{4(aq)}$ (Merck; >99.0%), $Mg(NO_3)_2.6H_2O$ (Merck; >99.0%), and 1.0 M K_2CO_3 (Merck; >99.7%). Table 1 represents the amount used as the precipitant: 1 M K_2CO_3. Firstly, the sample was washed in warm water after the filtration of the precipitant. Next, dried the sample at 120 °C for 12 h. After that, the precipitant was pre-calcinated in the air at 500 °C for 5 h to remove CO_2. Then, pressed the sample into discs at 600 kg/m^2. Finally, the sample was calcined at 1150 °C for 20 h to im-

Table 1. Preparation of catalyst

Catalysts	Support (MgO) $Mg(NO_3)_2.6H_2O$ (g)	Promoter (ZrO_2) $ZrCl_4$ (g)	Total weight of MgO and ZrO_2 after calcine (g)	Impregnation of the main catalyst (1% Pt) (1% Pd) (1% Ni) (g)		
				$Pt(acac)_2$	$Pd(acac)_2$	$Ni(acac)_2$
Pt/MgO	25.0	0.0	1	0.02	0.029	0.044
Pt,Pd,Ni/$Mg_{0.97}Zr^{4+}_{0.03}O$	24.9	1.3	1	0.02	0.029	0.044
Pt,Pd,Ni/$Mg_{0.93}Zr^{4+}_{0.07}O$	23.8	3.0	1	0.02	0.029	0.044
Pt,Pd,Ni/$Mg_{0.85}Zr^{4+}_{0.15}O$	21.8	6.5	1	0.02	0.029	0.044

prove the mechanical properties and to ensure the MgO and ZrO_2 interacts smoothly.

Table 1 lists the steps involved in preparing the Pt,Pd,Ni(acac)$_2$/$Mg_{1-x}Zr_x$O catalysts (1 % concentrations of each Pt, Pd, and Ni metals). First, $Pt(C_5H_7O_2)_2.H_2O$ (Acros Chemicals; >99%) was used to impregnate 1 % Pt dissolved in dichloromethane for 5 h to produce Pt(acac)$_2$/$Mg_{1-x}Zr_x$O. Then, the catalyst was impregnated with 1 % of Pd and Ni each. $Pd(C_5H_7O_2)_2$ (Aldrich; >99.5 %) and $Ni(C_5H_7O_2)_2.H_2O$ (Acros Chemicals; >99 %) solutions in dichloromethane was used for 5 h for the preparation of the catalysts. The catalysts were dried at 120 °C for 12 h after impregnation in the air. Finally, the catalysts are grind and sieved into particles of sizes 80-150 or 150-250 μm in diameter.

2.2 Characterization catalyst

A diffractometer (Shimadzu model XRD 6000) was used, The radiation process took place in a Philips glass diffraction X-ray tube of broad focus 2.7 kW. The calculation of the size of the crystals is based on the Debye-Scherrer relationship [13].

The Kratos Axis Ultra DLD system is fixed with a monochromatic Al Kα (1486.6 eV) and two X-ray sources (Al & Mg). The operation of the X-ray gun, which is the source of excitation, is based on an emission current of 20 mA combined with 15 kV voltages. The mode of operation for this hemispherical analyzer is based on fixed analyzer transmission (FAT) for wide and narrow scanning. The amount of the pass energy was fixed at 100 eV and 40 eV. The region of interest for the narrow scan and photoelectron signals Mg2p, Zr3d, Pd3d, Ni2d, Pt4f, and O1s correspond to each other. The carbon charging correction refers to the binding energy of 285 eV for adventitious carbon.

The evaluation of the catalysts active site was performed using the temperature programmed reduction (H_2-TPR) method that required hydrogen. The apparatus used to perform the evaluation was the Thermo Finnegan TPDRO 1100, attached with a thermal conductivity detector.

The total surface area of the catalyst was calculated using the Brunauer–Emmett–Teller (BET) method with nitrogen adsorption set at -196 °C. Meanwhile, the Thermo Fisher Scientific S.P.A (model: Surfer Analyzer) nitrogen adsorption-desorption analyzer was used for analysis.

The apparatus, transmission electron microscopy (TEM) (Hitachi H7100 TEM with an increasing voltage of 10 MV) was used to identify the crystal system and the catalysts homogeneity. The apparatus Mettler Toledo TG-DTA (Pt crucibles, Pt/Pt-Rh thermocouple) and a heating range of 50 to 1000 °C, was used to conduct thermogravimetric analysis (TGA).

2.3 Catalytic evaluations

Production of syngas (H_2/CO) as the model for the reforming of biogas was conducted using a fixed bed stainless steel micro-reactor (i.d. ϕ = 6 mm, h = 34 cm) during the catalytic evaluation for DRM. A mass flow gas controller (SIERRA instrument) and an online gas chromatography (GC) (Agilent 6890N; G 1540N) equipped with Varian capillary columns HP-PLOT/Q and HP-MOLSIV were connected to a reactor.

Before the start of the process, the reduction of approximately 0.02 g of the catalyst was conducted by flowing 5 % H_2/Ar at 700 °C, and the holding period was 3 h. The aim of the reduction step was to convert the (Ni^{2+},Pd^{2+}, and Pt^{2+}) phase of the catalyst to the metal (Ni°, Pd°, and Pt°) phase at the active sites of the catalysts. The tested catalyst was held in a vertical position using plugs of quartz wool in the middle of a reactor. A thermocouple was placed into the catalyst chamber to control and check the reaction temperature. The calculations of the conversions for CH_4 and CO_2, selectivity for H_2 and CO, as well as ratios for syngas (H_2/CO), were based on Equations (2-6).

$$CH_4\ Conversion\ \% = \frac{CH_{4(in)} - CH_{4(out)}}{CH_{4(in)}} x100 \quad (2)$$

$$CO_2\ Conversion\% = \frac{CO_{2(in)} - CO_{2(out)}}{CO_{2(in)}} x100 \quad (3)$$

$$H_2\ Selectivity\ \% = \frac{H_2}{2\left[CH_{4(in)} - CH_{4(out)}\right]} x100 \quad (4)$$

$$CO\ Selectivity\ \% = \frac{CO}{\left[CH_{4(in)} - CH_{4(out)}\right] + \left[CO_{2(in)} - CO_{2(out)}\right]} x100 \quad (5)$$

$$\frac{H_2}{CO} ratio = \frac{H_2\ Selectivity\ \%}{CO\ Selectivity\ \%} \quad (6)$$

3. Results and Discussion

3.1 Characterization of the catalysts

3.1.1 XRD patterns

Figures 1 (a-d) display the XRD patterns of the catalysts with MgO and ZrO_2 contents. The

diffraction peaks were observed at 2θ = 37.0° (111), 42.9° (200), 62.3° (220), 74.7° (311), and 79.1° (222). This occurrence was related to the cubic form of magnesia (JCPDS file no.: 00-002-1207). Meanwhile, the peaks recorded at 2θ = 17.5° (100), 24.1° (211), 28.3° (111), 31.5° (111), 34.2° (020), 35.4° (102), 38.6° (120), 40.8° (102), 44.8° (211), 49.3° (220), 54.1° (122), 57.9° (222), 59.8° (120), 62.3° (311), 69.0° (123), and 74.7° (140) were attributed to the cubic form of zirconia (JCPDS file no.: 00-001-0750). The peaks that were recorded at 2θ = 24.4° (113), 30.3° (006), 36.0° (033), 41.4° (027), 45.6° (127), 50.7° (218), 56.3° (234), 56.0° (502), 57.2° (330), 62.5° (424), 65.7° (154), 71.3° (131), and 72.7° (032) were mainly attributed to the cubic form of the catalyst complex (Mg–Zr–O). As for the catalyst with 1 % Pt, Pd, and Ni for all the patterns, no diffraction peaks were observed. This observation is attributed to the catalyst containing an insubstantial amount of the metals. This observation was similar to the findings by Grange [14].

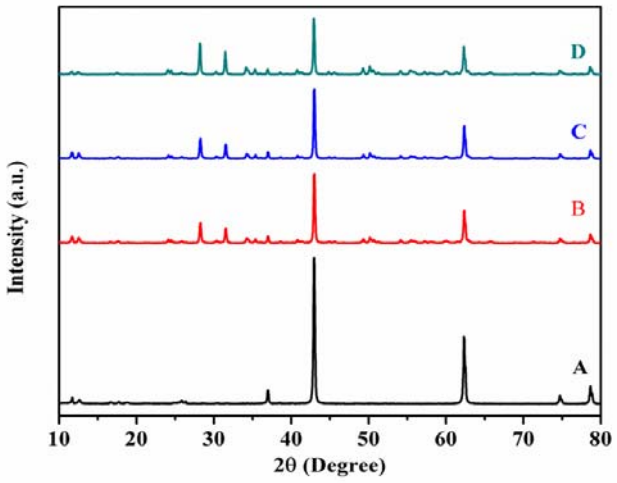

Figure 1. XRD patterns of the catalysts: (a) Pt,Pd,Ni/MgO, (b) Pt,Pd,Ni/$Mg_{0.97}Zr^{4+}_{0.03}O$, (c) Pt,Pd,Ni/$Mg_{0.93}Zr^{4+}_{0.07}O$, (d) Pt,Pd,Ni/$Mg_{0.85}Zr^{4+}_{0.15}O$

The Debye-Scherrer equation (Table 2) was used to calculate the diffraction of the highest peak in the XRD patterns. Later, this diffraction value was used to obtain the average crystalline size. The results showed that the size of the crystal and the increasing amount of zirconia in the catalysts was inversely proportional. This occurrence is attributed to the growth of magnesia crystallites due to the effects of the remains of Pt, Pd, and Ni on the sample surface. The size of the crystal was observed at 42.2, 47.7, 45.8, and 43.9 nm for the following catalysts, respectively:

- Pt,Pd,Ni/MgO (type 1)
- Pt,Pd,Ni/$Mg_{0.97}Zr^{4+}_{0.03}O$ (type 2)
- Pt,Pd,Ni/$Mg_{0.93}Zr^{4+}_{0.07}O$ (type 3)
- Pt,Pd,Ni/$Mg_{0.85}Zr^{4+}_{0.15}O$ (type 4)

Hence, the cubic crystal system is the most predominant among all the samples. This finding is supported by cubic shaped particles that were observed by TEM and FESEM.

XRF was used for the analysis of elements for all the components in the catalyst. Table 2 lists the percentages of Ni, Pd, and Pt, which are slightly more than 1. This result was mainly attributed to the incomplete precipitation of magnesium and zirconium metal precursors during the process of coprecipitation [15,16].

3.1.2 XPS analysis

Figures 2(a-g) illustrates the use of X-ray photoelectron spectroscopy (XPS) for the investigation of wide scan, O1s, Mg2p, Zr3d, Ni2p, Pd3d, and Pt4f of the reduced catalyst Pt,Pd,Ni/$Mg_{0.85}Zr_{0.15}O$. The following reveals the findings of a study, in which the spectra of the XPS on the surface of a few layers of the catalyst measure 3-12 nm. Figure 2a shows the wide scan of the catalyst, whereas, Figure 2b illustrates five significant oxygen species for O1s. These species are found on the topmost layer of the catalyst assigned to Ni–O, Zr–O, Mg–O, Pt–O, and Pd–O at binding energies of 528.1, 529.0, 531.9, 533.2, and 534.3 eV, re-

Table 2. Particle size measurement by XRD, TEM and XRF results

Catalysts	TEM (nm)	Crystal size (D) Debye-Sherrer eq. (nm)	Ni%	Pd%	Pt%	Mg & Zr%
Pt,Pd,Ni/MgO	49	42.2	1.13	1.09	1.15	95.50
Pt,Pd,Ni/$Mg_{0.97}Zr^{4+}_{0.03}O$	60	47.7	1.18	0.91	1.14	96.33
Pt,Pd,Ni/$Mg_{0.93}Zr^{4+}_{0.07}O$	53	45.8	1.03	1.13	1.18	96.2
Pt,Pd,Ni/$Mg_{0.85}Zr^{4+}_{0.15}O$	47	43.9	0.93	0.89	1.07	95.9

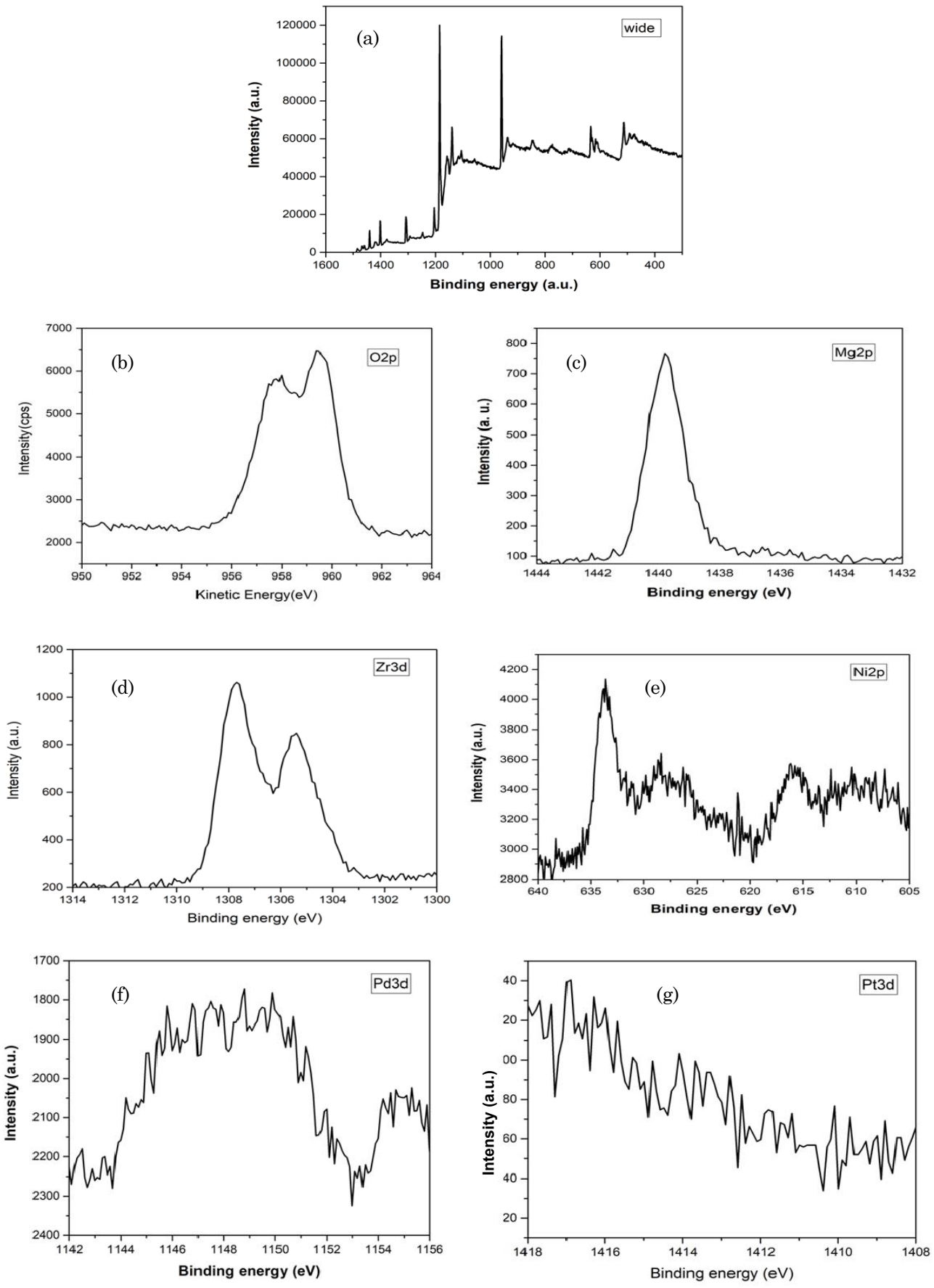

Figure 2. XPS narrow scans of the reduced catalyst: a) wide scan, b) O1s, c) Mg2p, d) Zr3d, e) Ni2p, f) Pd3d, g) Pt4f

spectively. Figure 2c shows one significant peak, obtained from Mg2p, bulk Mg–O at a binding energy of 49 eV. Meanwhile, Figure 3d provides an illustration of Zr3d of ZrO_2, with BE from 924 eV to 875.2 eV. The most intense photoelectron signal is that of Zr–O, which lies in the high BE region. The peaks are observed at 887.3 eV and 882.4 eV. The width of the $Ni2p_{3/2}$ spectrum is 29 eV, consisting of four main peaks due to the presence of Ni–O (Figure 2e). Four peaks are present in Pt4f and two peaks forPd3d , which is due to the presence of $Pt4f_{5/2}$ and $Pt4f_{7/2}$ that appear in the range of 74-66 eV in the catalyst (Figures 2 e-f) [17,18].

3.1.3 H_2-TPR

The TPR analysis were carried out on the following catalysts to examine their reduction behavior:

- Pt,Pd,Ni/MgO (type 1)
- Pt,Pd,Ni/$Mg_{0.97}Zr^{4+}_{0.03}O$ (type 2)
- Pt,Pd,Ni/$Mg_{0.93}Zr^{4+}_{0.07}O$ (type 3)
- Pt,Pd,Ni/$Mg_{0.85}Zr^{4+}_{0.15}O$ (type 4)

Figures 3(a-d) and Table 3 illustrate the TPR profiles of these catalysts. Figure 3a illustrates three well-defined reduction peaks in the TPR profile of the Pt,Pd,Ni/MgO. The first reduction peak is shown at 130 °C. This result is related to the reduction of the PtO species when Pt° is being produced, in comparison with a study conducted by Mahoney *et al.* [19] who detected the reduction of the PtO species at 114 °C. The second reduction peak, which is recorded at 184 °C, is due to the reduction of PdO to Pd°. The third and last peak is recorded within the region with a temperature of 511 °C due to the strong interaction of the supporting material to produce Ni. This is possible as the NiO species are very few. In a study conducted by Bao *et al.* [20], a reduction was observed in the NiO for the catalyst of Ni/ZrMgAl at 516 °C.

Figures 3(b-d) and Table 3 provide the TPR profile for catalysts including the ZrO_2 promoter. The TPR profiles of the catalysts (Type 2, 3, and 4) are not similar to that of the catalyst of Pt,Pd,Ni/MgO. One of the differences depends on the number of peaks. Results show five peaks. The first three peaks of the Pt,Pd,Ni/$Mg_{0.97}Zr^{4+}_{0.03}O$ catalyst were recorded at 115, 173, and 495 °C. Peaks of the Pt,Pd,Ni/$Mg_{0.93}Zr^{4+}_{0.07}O$ catalyst were shown at 123, 204, and 473 °C, while peaks of the Pt,Pd,Ni/$Mg_{0.85}Zr_{0.15}O$ catalyst were observed at 170, 192, and 484 °C. This condition is due to the reduction of PtO, PdO, and NiO that occurred on the top most layer of catalysts in obtaining the Pt°, Pd°, and Ni° elements, respectively. The fourth peak for the catalysts (Type 2, 3, and 4) was recorded when the temperatures were 532, 545, and 559 °C, respectively. The findings corresponded to the reduced amount of ZrO_2 on the surface. Thus, when the temperature of the catalysts dropped, a significant lowering was observed on the ZrO_2 surface. A few reasons for this occurrence were as follows: The first reason could be linked to the well-dispersed ZrO_2 particles during the process of incorporation of MgO into ZrO_2 and the retardation of sintering [21]. The other reason could be due to the occurrence when ZrO_2 and Pt, Pd, and Ni metals interact actively during the overlapping of PtO, PdO, NiO, and ZrO_2 in reducing the peaks. The fifth peak was formed at 635, 652, and 677 °C, respectively. Strong interactions exist between the species of the

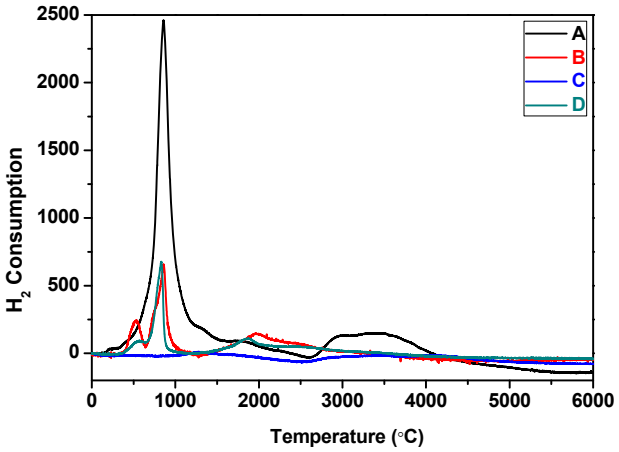

Figure 3. H_2-TPR profiles of catalysts reduced in a (5 % H_2/Ar) stream at a temperature ramp of 10 °C/min

Table 3. H_2-TPR values of the different catalysts

Catalysts	Temp. °C	Temp. °C	Temp. °C	Temp. °C	Temp. °C	Amount of Adsorbed H_2 gas (µmol/g)
Pt,Pd,Ni/MgO	130	184	511	-	-	488.6
Pt,Pd,Ni/$Mg_{0.97}Zr^{4+}_{0.03}O$	115	173	495	532	635	503.7
Pt,Pd,Ni/$Mg_{0.93}Zr^{4+}_{0.07}O$	123	204	473	545	652	517.9
Pt,Pd,Ni/$Mg_{0.85}Zr^{4+}_{0.15}O$	170	192	484	559	677	523.4

ZrO_2 promoter and the MgO support with the reduction of bulk ZrO_2. Catalysts showed a higher degree of reducibility when the loading of the promoter increased. This finding was similar to results obtained from previous studies. Rotaru *et al.* [21] reported that the reduction of zirconium occurred at 490 and 790 °C. Their findings also revealed that the promoters were well-dispersed for the support, and the interaction between the support with doping Pt, Pd, and Ni species was high. The other finding stated that the significant peak of TPR profile was formed at temperatures ranging from 684 °C to 737 °C. Thus, ZrO_2 alone was capable of reducing the range in temperatures [22]. Another obvious finding pointed out that the addition of the ZrO_2 promoter was effective in the reducibility of catalysts with MgO support. $Mg_{1-x}Zr^{4+}{}_xO$, which recorded a higher basicity than MgO, showed more interaction with the ZrO_2 promoter. Consequently, PtO, PdO, and NiO were reduced more significantly because of the redox property of $Mg_{1-x}Zr^{4+}{}_xO$ [23].

The total amount of H_2 consumed during the reduction of the catalysts (type 1, 2, 3, and 4) was calculated from the total peak area. The calculations for these catalysts were recorded at 488.6, 503.7, 517.9, and 523.4 μmol/g catalyst, respectively. According to H_2-TPR results, the most active catalyst was $Pt,Pd,Ni/Mg_{0.85}Zr^{4+}{}_{0.15}O$, which suggests that it was the most suitable catalyst for DRM reaction.

3.1.4 BET surface area

Table 4 tabulates the surface area, pore radius, and pore volume of the support MgO and for the $Pt,Pd,Ni/Mg_{1-x}Zr_xO$ catalysts (where x = 0.00, 0.03, 0.07, and 0.15). The surface area for Pt,Pd,Ni/MgO catalyst with a cubic structure supported with TEM was recorded at 12.4 m^2/g, while the surface area for the support MgO was recorded at 11.1 m^2/g. The former recorded a higher value because of the consequences of the Pt, Pd, and Ni loadings on the specific surface area of the MgO support. In such cases, the surface areas of Pt,Pd,Ni/MgO catalyst was substantially smaller than that of the conventional catalyst (type 2, 3, and 4) which were at 16.7, 17.1, and 18.9 m^2/g, respectively. The main reason was the presence of layers of Pt, Pd, and Ni particle partially covering the magnesia pores. The BET surface area of MgO that was promoted by ZrO_2 was nearly similar to one of the common Pt, Pd, and Ni catalysts with binary support [24]. Meanwhile, the features of the supported Pt, Pd, and Ni catalysts with a cubic structure revealed very low metal dispersion and small surface areas of Pt and Pd with few Ni particles. This occurrence is due to the highly interactive activity between the layers of Pt, Pd, and Ni and the support of MgO with the ZrO_2 promoter. The pore volume of $Pt,Pd,Ni/Mg_{0.85}Zr^{4+}{}_{0.15}O$ catalyst was 0.19 cm^3/g. This value was slightly higher than that of $Pt,Pd,Ni/Mg_{0.97}Zr^{4+}{}_{0.03}O$ and $Pt,Pd,Ni/Mg_{0.93}Zr^{4+}{}_{0.07}O$ catalysts, which were 0.11 and 0.18 cm^3/g, respectively. This finding was different from the study of Bao *et al.* [20], where the pore volume of NiCeMgAl catalyst was 0.51 cm^3/g.

Table 4 illustrates the pore radius of various catalysts. The pore size of the support MgO was 9.9 Å; whereas, the pore size of Pt,Pd,Ni/MgO catalyst was 9.7 Å. The pore radius of the other catalysts and the increase of the ZrO_2 promoter in the support were inversely proportionate to one another. The pore radii of the catalysts (type 2, 3, and 4) were 23.9 Å, 23.5 Å, and 23.2 Å, respectively [25]. These data showed that $Pt,Pd,Ni/Mg_{0.85}Zr_{0.15}O$ catalyst with a high surface area recorded better performance in the DRM reaction compared with other catalysts.

Table 4. The main textural properties of fresh catalysts

Sample name	Specific surface area (m^2/g)	Pore volume (cm^3/g)	Pore radius (Å)
MgO	11.1	0.21	9.9
Pt,Pd,Ni/MgO (type 1)	12.4	0.21	9.7
$Pt,Pd,Ni/Mg_{0.97}Zr^{4+}{}_{0.03}O$ (type 2)	16.7	0.11	23.9
$Pt,Pd,Ni/Mg_{0.93}Zr^{4+}{}_{0.07}O$ (type 3)	17.1	0.18	23.5
$Pt,Pd,Ni/Mg_{0.85}Zr^{4+}{}_{0.15}O$ (type 4)	18.9	0.19	23.2
Spent catalyst	19.3	0.14	24.7

3.1.5 TEM characterization

Figures 4(a-d) show TEM images of Pt,Pd,Ni/MgO (type 1), Pt,Pd,Ni/$Mg_{0.97}Zr^{4+}_{0.03}O$ (type 2), Pt,Pd,Ni/$Mg_{0.93}Zr^{4+}_{0.07}O$ (type 3), and Pt,Pd,Ni/$Mg_{0.85}Zr^{4+}_{0.15}O$ (type 4) catalysts with cubic structures. The catalysts underwent calcination at 1150 °C with uniformity in the distribution of particles but without free ZrO_2. Figures 4(b-d) confirms the formation of MgO-ZrO_2 solid solutions [26] with cubic oxide particles on the Pt, Pd, and Ni layers of the supported metal. The Pt,Pd,Ni/$Mg_{0.85}Zr^{4+}_{0.15}O$ catalyst (Figure 4d) dispersed 1% of the Pt, Pd, and Ni metal particles each for the support magnesia-zirconia of sizes between 45 to 85 nm [27]. In addition, TEM analysis of the Pt,Pd,Ni/$Mg_{0.85}Zr^{4+}_{0.15}O$ catalyst indicated an induced growth with an agglomeration of the nanoparticles at a specific distance between the metal crystallites. Often, this type of growth was catalyzed by metallic platinum, palladium, and nickel, although the distribution of TEM image sizes showed more realism

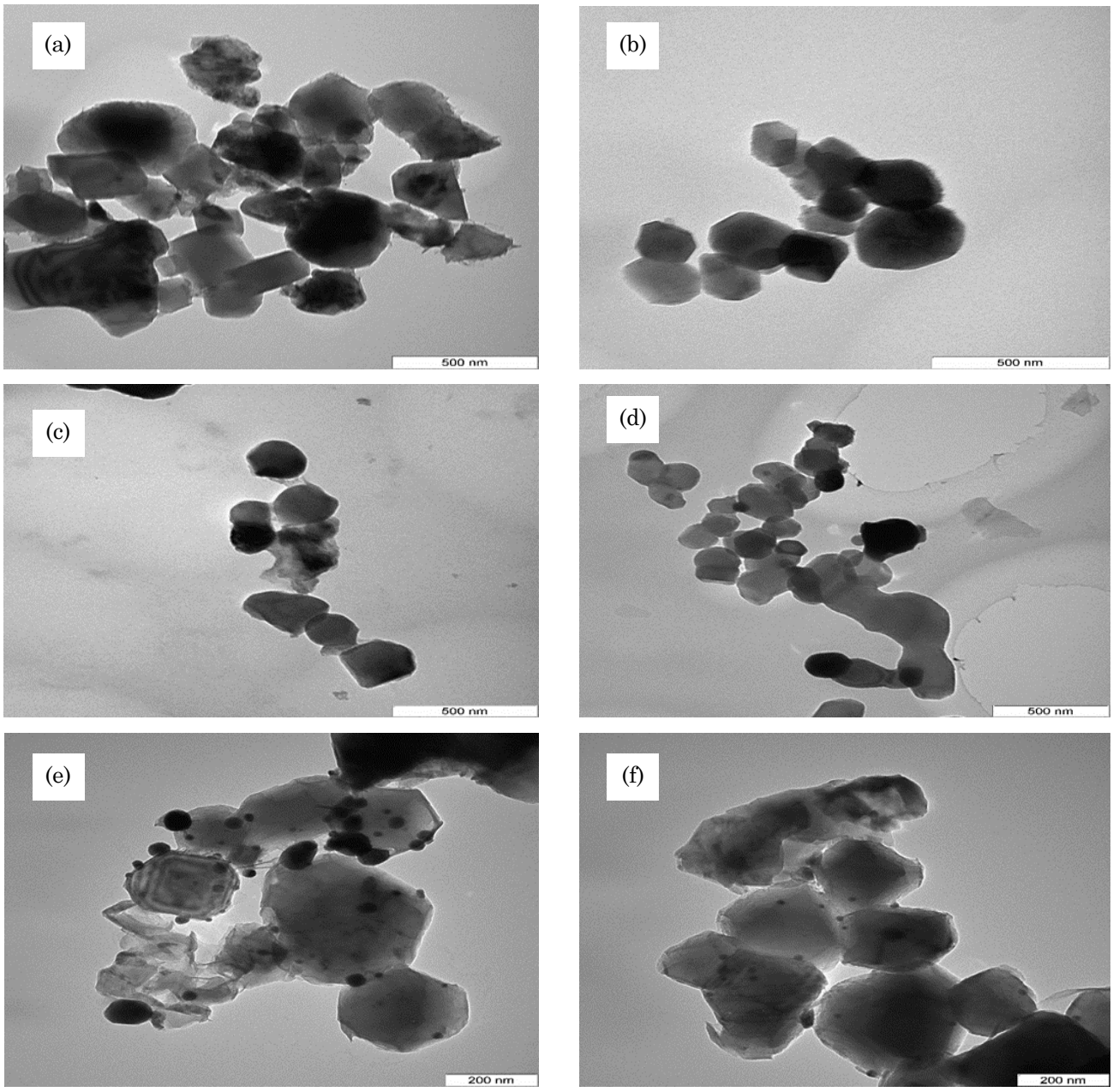

Figure 4. TEM image of catalysts: (a) Unreduced Pt,Pd,Ni/MgO, (b) Unreduced Pt,Pd,Ni/$Mg_{0.97}Zr^{4+}_{0.03}O$, (c) Unreduced Pt,Pd,Ni/$Mg_{0.93}Zr^{4+}_{07}O$, (d) Unreduced Pt,Pd,Ni/$Mg_{0.85}Zr^{3+}_{15}O$, (e) Reduced Pt,Pd,Ni/$Mg_{0.93}Zr^{4+}_{07}O$ with 5 % H_2 in Ar at 700 ^oC, (f) Pt,Pd,Ni/$Mg_{0.93}Zr^{4+}_{0.07}O$ after 200 h reaction, at 900 ^oC, and CH_4/CO_2 ratio 1:1.

and accuracy [28]. Figures 4(a-e) show the TEM results, which are in agreement with XRD data. These results showed that Mg–Zr–O was not only complex but also cubical, similar to MgO and ZrO_2.

3.1.6 Thermal analysis

Figures 5(a-d) show TGA for the Pt,Pd,Ni/MgO (type 1), Pt,Pd,Ni/$Mg_{0.97}Zr^{4+}_{0.03}O$ (type 2), Pt,Pd,Ni/$Mg_{0.93}Zr^{4+}_{0.07}O$ (type 3), and Pt,Pd,Ni/ $Mg_{0.85}Zr^{4+}_{0.15}O$ (type 4) catalysts. Results indicated a weight loss, however, it occurred at only one phase of the thermal process. The amount of weight loss was approximately 4 % at temperatures ranging from 100 to 120 °C. This effect was due to the removal of moisture from the Pt,Pd,Ni/$Mg_{1-x}Zr_xO$ catalyst. On one hand, the catalysts (type 1, 2, 3, and 4) involve weight loss at 2.5, 2.3, 2.6, and 2.7%, respectively. On the other hand, Pt,Pd,Ni/$Mg_{0.85}Zr^{4+}_{0.15}O$ (type 4) and Pt,Pd,Ni/$Mg_{0.93}Zr^{4+}_{0.07}O$ (type 3) catalysts (See Figures 5(c-d)) showed further weight loss at 2.3 % and 2.7 %, respectively, at the second stage. This effect was due to the oxygen atoms removed from the catalyst. From the graph, the initial findings revealed that the entire weight of the compound showed a slight increase, because the compound adsorbs the N_2 gas in the machine. All the compounds remained stable at 600 °C. This result was attributed to the high melting point of magnesia and zirconia at 2852 and 2177 °C, respectively. From Figures 5(a-d), the components of the catalyst interacted well with one another. These findings are similar with the results obtained by Mojovic *et al.* [29].

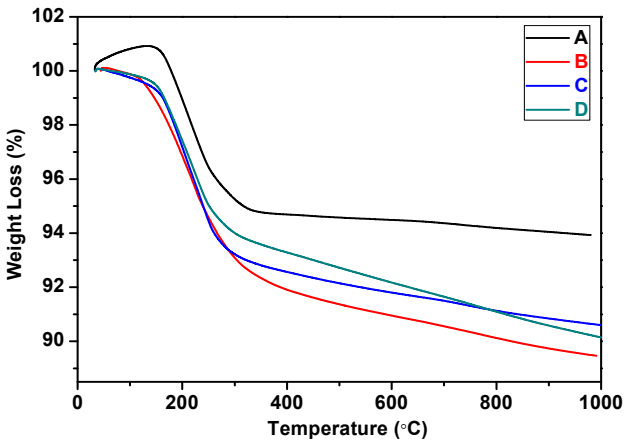

Figure 5. TG of the catalysts:
(a) Pt,Pd,Ni/$Mg_{0.97}Zr^{4+}_{0.03}O$, (b) Pt,Pd,Ni/MgO,
(c) Pt,Pd,Ni/$Mg_{0.8}Zr^{4+}_{0.15}O$,
(d) Pt,Pd,Ni/$Mg_{0.93}$ $Zr^{4+}_{0.07}O$

3.2 Catalytic performance in biogas reforming

3.2.1 Effects of reactant concentration on conversion

The conversion of CH_4 and CO_2 indicates the reactive activity of the DRM, while the H_2/CO ratio expresses the selectivity. The blank test results, where no catalyst was used, indicated the H_2 and CO presence in the outlet gas when the temperature was set above 900 °C. This occurrence resulted from the decomposition of methane (Equation 7). When $Mg_{1-x}Zr_xO$ was used in the absence of other metals, the conversion of CH_4 and CO_2 was very low, with recording of 36 % and 50 %, respectively; whereas, the H_2/CO ratio was recorded at 0.3 %. These findings indicate a weak reaction occurred in the pores of the support promoter. Meanwhile, BET results also revealed similarity; the presence of pores in the catalyst. On the contrary, an increase in the conversion of CH_4 and CO_2 and the H_2/CO ratio was observed (Figure 6) when Pt,Pd,Ni/$Mg_{1-x}Zr^{4+}{}_xO$ catalysts were used. Hence, Pt, Pd, and Ni metals doped on the support have a significant effect in the catalytic reaction. Pt,Pd,Ni/$Mg_{0.85}Zr^{4+}_{0.15}O$ (type 4) catalyst recorded CH_4 and CO_2 conversion of 91 % and 99 %, respectively, in the 1:1 ratio for CH_4:CO_2 and 1.28 for H_2:CO ratio. The conversion of the gases recorded CH_4 and CO_2 conversion of 85 % and 96 %, respectively, in the reactant ratio (2:1) and 1.16 for H_2:CO ratio. These findings revealed that the 1:1 ratio is the most effective in resisting the deactivation of the catalyst for carbon deposition and high selectivity of H_2

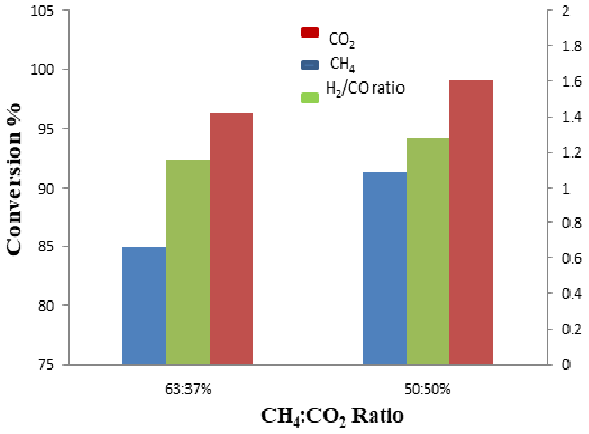

Figure 6. The effect of changing the ratio concentration of CH_4: CO_2 reactant 1- 2:1 and 2-1:1 over the % of their conversion and H_2/CO ratio for Pt,Pd,Ni/$Mg_{0.85}Zr^{4+}_{0.15}O$ catalyst at 900 °C

and CO (Figure 6). Meanwhile, the remaining catalysts are similar in this characteristic [30].

$$CH_4 \rightarrow C + 2H_2 \quad \Delta H_{298^o} = 75.0 \text{ kJ/mol} \qquad (7)$$

3.2.2 Effects of concentration of catalyst on conversion

Figure 7 and Table 5 illustrate the consequences of varying concentration levels of the catalyst during the conversion process. The conversion of CH_4, CO_2, and the H_2/CO ratio showed that the catalysts were arranged in an order, where Pt,Pd,Ni/MgO < Pt,Pd,Ni/$Mg_{0.97}Zr^{4+}_{0.03}O$ < Pt,Pd,Ni/$Mg_{0.93}Zr^{4+}_{0.07}O$ < Pt,Pd,Ni/$Mg_{0.85}Zr^{4+}_{0.15}O$. The main catalysts, namely, Pt and Pd with Ni and the support, MgO-ZrO_3 were combined together. Experiments were conducted at 900 °C and 1 atm with a 1:1 reactant ratio (CH_4:CO_2) (Figure 7 and Table 5). In the conversion of methane, the highest reading was recorded for the Pt,Pd,Ni/$Mg_{0.85}Zr^{4+}_{0.15}O$ (91 %) catalyst; whereas, the lowest reading was found in the Pt,Pd,Ni/MgO (75 %) catalyst. The other finding revealed that many catalysts that were tested showed a slight deactivation after 200 h.

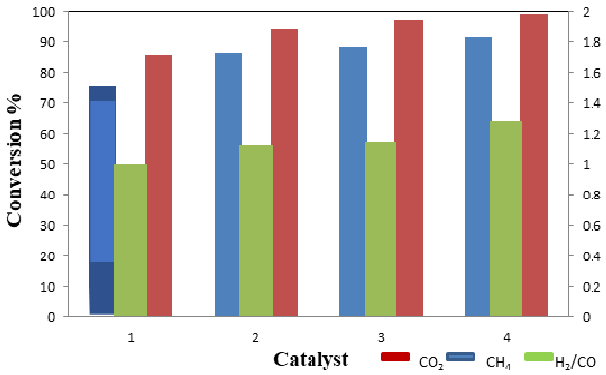

Figure 7. The effect of using different catalysts 1) Pt,Pd,Ni/MgO, 2) Pt,Pd,Ni /$Mg_{0.97}Zr^{4+}_{0.03}O$, 3) Pt,Pd,Ni/$Mg_{0.93}Zr^{4+}_{0.07}O$, and 4) Pt,Pd,Ni/$Mg_{0.85}Zr^{4+}_{0.15}O$ on CH_4, CO_2 conversion and H_2/CO ratio at 900 °C for the 1:1 ratio of CH_4:CO_2

In general, the CO_2 conversion recorded more stability than the CH_4 conversion. As for the conversion of CO_2, the Pt,Pd,Ni/$Mg_{0.85}Zr^{4+}_{0.15}O$ (99 %) catalyst provided the highest rate of conversion; whereas, the Pt,Pd,Ni/MgO (86 %) catalyst revealed the lowest rate of conversion. These results showed that the catalyst of Pt,Pd,Ni/$Mg_{0.85}Zr^{4+}_{0.15}O$ is the most effective catalyst in the conversion process.

The value of the product ratio of H_2/CO for catalysts (Figure 7 and Table 5) was more than 1. These findings indicated that the process of CO_2 conversion of Ni metal showed less favorable results than that of the tri-metallic catalysts compared with a previous study [20]. However, an evidence of improvements was observed in the side reactions indicated by the differences between the conversions and the product yields. Table 5 presents evidence that an increase in the concentration level of zirconia was followed by an increase in the conversion rate of CH_4 and CO_2 as well as the H_2/CO ratio. The Pt,Pd,Ni/$Mg_{0.85}Zr^{4+}_{0.15}O$ catalyst produces an excellent result at the site with most activity of H_2-TPR and it also produced the outstanding BET result from the large surface area.

This occurrence reveals that the addition of ZrO_2 into the MgO catalysts can significantly reduce the reverse water-gas shift (RWGS) reaction (Equation 8).

$$CO_2 + H_2 \rightarrow CO + H_2O \quad \Delta H_{298^o}=41.0 \text{ kJ/mol} \quad (8)$$

Results also indicated that the CO formation rate in the DRM reaction depended on the strong interaction between the ZrO_2 promoter and the support MgO in solid solution. The findings are as follows: the ratio of mole in the catalyst is 0.15:0.85, the biggest surface area is 18.9 m^2/g (Table 4), and the site with the most activity has 523.4 µmol/g from the total amount of H_2-consumption provided evidence for H_2-TPR study (Table 3). Thus, the process of forming a solid solution was important in the production of active sites for the CO_2 reforming of methane.

Table 5. The catalytic results of DRM reaction for the catalysts at 900 °C for the 1:1 ratio of CH_4:CO_2

Catalysts	CH_4 Conversion %	CO_2 Conversion %	H_2/CO ratio
Pt,Pd,Ni/MgO	75	86	1.07
Pt,Pd,Ni/$Mg_{0.97}Zr^{4+}_{0.03}O$	86	94	1.12
Pt,Pd,Ni/$Mg_{0.93}$ $Zr^{4+}_{0.07}O$	88	97	1.15
Pt,Pd,Ni/$Mg_{0.85}$ $Zr^{4+}_{0.15}O$	91	99	1.28

The presence of the entire ZrO_2 promoter as a solid solution stabilized the two oxides. When hydrogen was reduced at 700 °C, only the surface layer of the ZrO_2 solid solution of the ZrO_2-MgO catalyst was shrunk. Moreover, the Zr sites produced remained close to the solid solution, thereby causing an obstacle to Zr sintering [31]. Moreover, the sites that affected the catalytic process were found in the Pt, Pd, and Ni particles causing abundant interaction between the Pt, Pd, and Ni particles and MgO-ZrO_2. When the Pt, Pd, and Ni concentration levels in the support increased, the CH_4 and CO_2 conversion and selectivity did not show any significant change. This occurrence could be due to the formation of nanoparticles, which is the consequence of the XRD (Debye Sherrer's equation) and TEM results (Table 2).

Despite the use of X-ray diffraction for a simplistic and possible estimation of the crystal size from the widening of the XRD reflections through the use of Scherrer's formula, the nanoparticulation of the particles was preferred. The nanoparticles selected as catalysts for this study maximized the surface area and secured more reactions. Moreover, these catalysts allowed the Pt, Pd, and Ni metals to be dispersed effectively on the surface of the catalysts. These catalysts also provided strong Lewis basicity with metal oxide support. Furthermore, the increase in the support for Lewis basicity enhanced the ability of the catalyst to chemisorb CO_2 in the DRM reaction. Subsequently, the formation of CO occurred when the adsorbed CO_2 reacted with deposited carbon (Equation 9) with less formation of coke.

$$CO_2 + C \rightarrow 2CO \quad \Delta H_{298^o}=+172 \text{ kJ/mol} \qquad (9)$$

XPS results suggested the use of a special approach, which is the formation of the ZrO_2-MgO solid solution, to prevent carbon deposition. MgO is a strong Lewis base and has a high adsorption of CO_2 in the reduction or prevention of carbon deposition. Besides, the reduction of ZrO_2 in the ZrO_2-MgO solid solution was more difficult, often causing the smaller particles of zirconium to be formed on the topmost layer compared with that of unadulterated ZrO_2 [32,33]. When surface basicity combines with the particle size of small metals, the MgO-based solid solution catalyst can prevent carbon deposition more effectively. Despite a more realistic and accurate distribution of TEM images in terms of size, several drawbacks existed in the images.

The high readings in the conversion of CH_4 and CO_2 were due to the involvement of the particle size in the reactive activity which recorded the best result. Moreover, the preparation of Pt, Pd, and Ni doping metals was based on the Debye-Sherrer equation and the support of TEM analysis. The metal size was as nanoparticles. Therefore, the particle size is crucial in the activity of the reaction. Another findings reported that when the size of the particles had been reduced to nano range, an increase in the conversion of the reactants and selectivity was observed. This result was supported by findings of more activities which were recorded at 523.4 μmol/g in the active sites and at 18.9 m^2/g in the surface area (Tables 3 and 4).

3.2.3 Effects of temperature on conversion

Figure 8 presents the results of the selectivity and activity of Pd,Pd,Ni/$Mg_{0.85}Zr^{4+}_{0.15}O$ catalyst from 700 to 900 °C. The conversion of CH_4:CO_2 (1:1) increased when the temperature was raised from 700 to 900 °C. During the DRM, the strong endothermic reaction (Equation 1) and a higher increase in temperature in the conversion rate have contributed to the increase in the conversion ratio of CH_4:CO_2. This occurrence has been reported in earlier research [34]. The CH_4 conversion of Pd,Pd,Ni/$Mg_{0.85}Zr^{4+}_{0.15}O$ increased from 45 to 91 % when the temperature was raised from 700 to 900 °C. Meanwhile, the CO_2 conversion increased from 56 to 99 %. For temperatures of more than 900 °C, no significant increase occurred in the CH_4 and CO_2 conversions. Figure 8 shows the H_2/CO ratio of the catalyst for different temperatures. When the temperature was <900 °C, the H_2/CO ratio of the samples was <1. This occurrence was due to the RWGS (Equation 8) that consumed more H_2 and simultaneously produced CO, resulting in the lowering of H_2/CO ratio. The H_2/CO ratio of Pd,Pd,Ni/$Mg_{0.85}Zr^{4+}_{0.15}O$ was 1.28 when the temperature was 900 °C. This result indicates that the RWGS reaction (Equation 8) causes slight effect [7] because the concentration of hydrogen will remain high while the concentration of carbon monoxide is low and therefore the H_2/CO ratio remains high.

3.2.4 Stability tests

Figure 9 presents the result obtained from the test involving temperature. Results showed that the CH_4 and CO_2 conversion rate was high at 900 °C. In this mechanism, the reaction between a molecule of methane and Ni surface (Nickel has the best conversion among other metals due to its size and high density of posi-

tive charge [10]) produced desorbed hydrogen and hydrocarbon species CH_x (x = 0-4); when x=0, carbon deposits on the Ni metal surface [35]. Equations 10-14 are shown below:

$$CH_4 + 2Ni_{(as)} \rightarrow CH_3Ni_{(as)} + HNi_{(as)} \quad (10)$$

$$CH_3Ni_{(as)} + Ni_{(as)} \rightarrow CH_2NI_{(as)} + HNi_{(as)} \quad (11)$$

$$CH_2Ni_{(as)} + Ni_{(as)} \rightarrow CHNi_{(as)} + HNi_{(as)} \quad (12)$$

$$CHNi_{(as)} + Ni_{(as)} \rightarrow CNi_{(as)} + HNi_{(as)} \quad (13)$$

$$2HNi_{(as)} \rightarrow H_2 + 2Ni_{(as)} \quad (14)$$

(as) metal active site

Nakamura *et al.* [36] described the effects of a promoter on the catalyst during the DRM through an increase in the dispersion of Pt, Pd, and Ni. One of the effects was the activation of carbon dioxide on the support-promoter that had been mixed with the metal particle for the formation of a carbonate species. Subsequently, the CH_x species reduced the carbonate substrate to form carbon monoxide (CO) (Equations 15-19).

$$CO_{2(g)} \rightarrow CO_{2(support)} \quad (15)$$

$$CO_{2(g)(support)} + O^{-2}_{(support)} \rightarrow CO_3^{-2}{}_{(support)} \quad (16)$$

$$2H_{(metal)} \rightarrow 2H_{(support)} \quad (17)$$

$$CO_3^{-2}{}_{(support)} + 2H_{(support)} \rightarrow HCO_2^{-1}{}_{(support)} + OH^{-1}{}_{(support)} \quad (18)$$

$$CO_{(support)} \rightarrow CO_{(g)} \quad (19)$$

As it is well known that carbon deposited on the metal surface will decrease the stability of the catalysis but the presence of ZrO_2 promoter will remove the deposited carbon and reactivated the catalyst. The presence of the ZrO_2 promoter in the catalyst was mainly to secure a very stable platform and strong resistance to coking that may occur when CO_2 and CH_4 are being converted as well as the H_2/CO ratio for reactions of 200 h or more. The carbon formed on the catalyst was removed by ZrO_2 during the DRM reaction. Moreover, the enhancement of CO_2 adsorption occurred in the presence of ZrO_2 because it can increase the basicity. This phenomenon was closely followed by the formation of carbonate species, particularly ZrO_2 that is capable of breaking down CO_2 into CO and O. Finally, the O atom is moved to Zr promoter. At the last stage, the O atom combined with the C that deposits on the metal catalyst had produced CO [37]. Based on the findings, a significant decline in the carbon deposition on the catalyst was observed (Equations 20-21).

$$CO_{2(g)} \rightarrow CO_{(support)} + O_{(promoter)} \quad (20)$$

$$C_{(metal)} + O_{(promoter)} \rightarrow CO_{2(g)} \quad (21)$$

In the case of a low ZrO_2 concentration, the CO_2 conversion indicated active formation of strong ionic oxides, such as $ZrOCO_3$, which attracted CO_2 to the topmost layer of the catalyst that subsequently increases the CH_4 conversion rate. In the case of a high ZrO_2 concentration, the conversion rate for both CH_4 and CO_2 declined. The decrease could be attributed to the higher electron density of Pt, Pd, and Ni [38]. The decomposition of the $ZrOCO_3$ species in DRM has produced CO and an oxygen species that react with the carbon deposits on the interface of Pt, Pd, and Ni-$ZrOCO_3$ thus reviving the activity sites of the Pt, Pd, and Ni. ZrO_2 supported catalysts similarly facilitated the dissociation of adsorbed CO_2. Besides its promotional effect on CO_2, the dissociative adsorption of zirconia has improved the dispersion

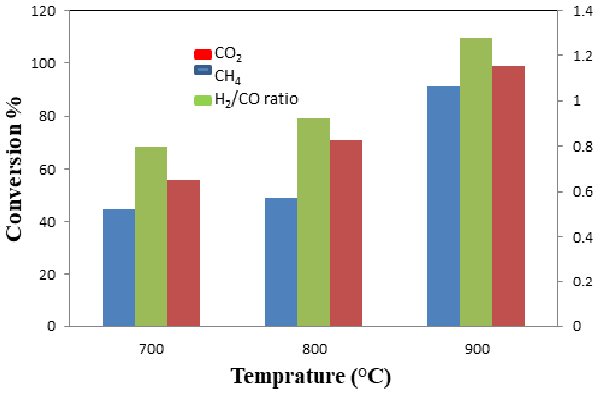

Figure 8. The influence of temperature on the catalytic activity of the Pt,Pd,Ni/$Mg_{0.85}Zr^{4+}{}_{0.15}O$ catalyst: 1) 700 °C, 2) 800 °C, 3) 900 °C for the 1:1 ratio of CH_4:CO_2

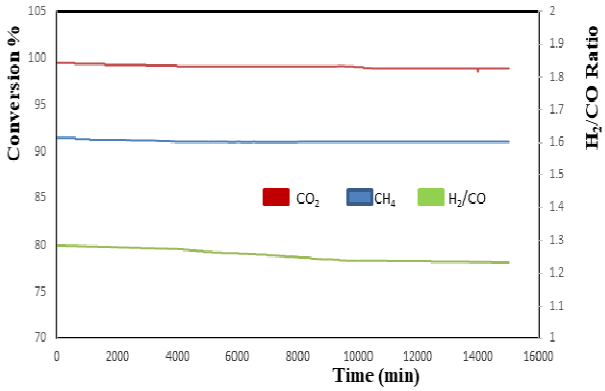

Figure 9. Stability tests of Pt,Pd,Ni/$Mg_{0.85}Zr^{4+}{}_{0.15}O$ catalysts at 900 °C for the 1:1 ratio of CH_4:CO_2, for 200 h. (GHSV = 15000 ml.gcat^{-1}.h^{-1}, atmospheric pressure)

and stabilization of small metal particles. In fact, zirconia is an oxide with proven ability to have strong interaction during the support metallic phase; hence, significant changes occurred in the surface properties of both the oxide and metal [39].

The activity and stability of the Ni, Pd, and Pt tri-metallic catalyst had better results than that of the mono-metallic Ni or Pd-Ni catalyst and Pt-Ni bi-metallic catalysts (Table 3 and Figure 8). This may have attributed to the fact that the Pd and Pt transfer the electron density to their Ni metal (main catalyst) in the tri-metallic catalyst, as described in our previous work (10). This result is consistent with the hypothesis that Pt and Pd can prevent the oxidation of Ni as its electron density increases [40,41]. When the Pt-Ni or Pd-Ni bi-metallic cluster is formed, the reducibility of Ni increased. In such cases, the activities for experiments of more than 200 h are higher and more stable [12,42].

3.2.5 Post-reaction characterization

TGA and TEM images indicated the presence of very low concentration of coke deposit of the spent catalyst. Figure 4f shows TEM images of the spent catalysts that reveal similar structure of the catalyst was intact even after it had undergone stream testing for 200 h. Moreover, no change occurred in the two-dimensional cubic texture of the spent catalyst. TEM results showed layered deposition of the carbon with no traces of filamentous carbon. However, the pore size of the spent catalyst showed a remarkable increase from 23.2 Å to 24.7 Å. BET analysis also revealed that the surface area of the spent catalyst had increased slightly from 18.9 to 19.3 m^2/g. A slight metal sintering was also observed in the spent catalyst. Although the cubic channel of the used catalyst indicated that the sintering of the active metals inside the pore was limited, the active metals that supported the outer surface experienced significant sintering. A negligible coke deposition occurred because of the absence of filamentous carbon in the used catalyst.

Figure 10 presents TGA with an oxygen stream of post-reaction of the catalyst Pt,Pd,Ni/$Mg_{0.85}Zr^{4+}_{0.15}O$, and the calculation of weight change for each temperature range with reference to the thermogram, three different regions with different ranges in temperature exist. The temperature range in the first region is low because of the weight increase in the spent catalyst. The temperature range in the second region is of mid-range, whereby the weight of the spent catalyst declined. The temperature range in the third region is of high range because of the weight increase in the spent catalyst. The weight increase is due to the oxidation of Ni particles at temperatures higher than 100 °C. Zhu *et al.* [43] reported that the weight increase in the spent catalyst was lower than 3%. The compound showed increased slightly when the temperature range was at 150-500 °C; whereas, the weight loss at 650 °C was due to the oxidation of deposited carbon.

The calculation of the coke deposition on the spent catalyst amounted to 1.6 wt %. Finally, all the elements on the topmost layer were oxidized by oxygen after removing the carbon found on the topmost layer as CO_2. Thus, it can be obtained at 900 °C. A very small amount of coke is deposited on the topmost layer of the

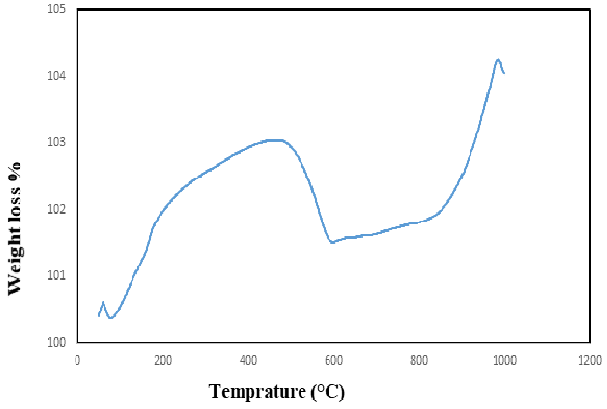

Figure 10. TGA profiles of spent Pt,Pd,Ni/$Mg_{0.85}Zr^{4+}_{0.15}O$ catalyst (20 mL/min O_2 stream under a temperature ramp of 10 °C/min)

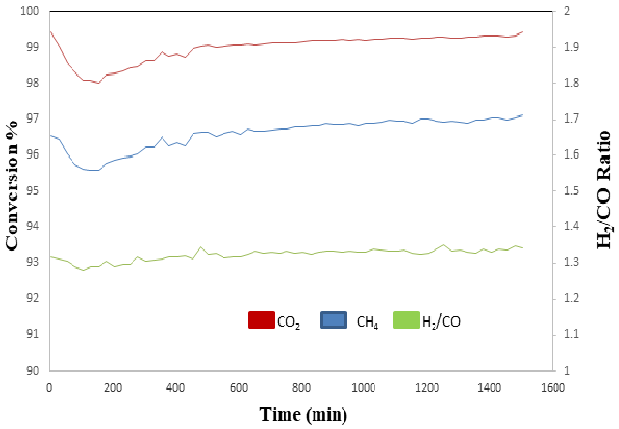

Figure 11. DRM reaction of the Pt,Pd,Ni/$Mg_{0.85}Zr^{4+}_{0.15}O$ catalyst under 900 °C with 1.25 % O_2

catalyst because of the good metals dispersed in the catalysts, and the smaller crystal metal catalysts do not deactivate easily because of their nanoparticle size.

3.2.6 Enhancing the catalyst

DRM reaction can be improved with experiments conducted in low oxygen concentration flow (1.25 %). Figure 11 presents data that show improvement in the conversion of CH_4 from 91 to 96 %. This improvement is achieved by adding an oxidant (O_2) to partially or completely oxidize methane together with the use of exothermicity in the reaction that supplies the necessary direct heat to the DRM reactant mixture [38]. However, this process does not affect the CO_2 conversion and the H_2/CO ratio because of the reaction between oxygen and CH_4 to produce CO and H_2O (Equation 22). This is followed by the reaction between the steam and the deposited carbon to produce syngas (Equation 23). Coke deposition is also reduced because of the presence of O_2 on the catalyst (Equation 24). Thus, this process has not only decreased the amount of carbon deposition but also improved the lifespan of the catalyst.

$$CH_4 + 1.5O_2 \rightarrow CO + 2H_2O_{(v)} \quad (22)$$

$$C_{(s)} + H_2O \rightarrow CO + H_2 \quad (23)$$

$$C_{(s)} + O_2 \rightarrow CO_2 \quad (24)$$

4. Conclusion

Dry reforming of methane over Ni,Pd,Pt/$Mg_{1-x}Zr_xO$ catalysts were carried out for the production of syngas. The catalysts were synthesized using co-precipitation method with K_2CO_3 as the precipitant. The catalysts were characterized for its physicochemical properties by XRD, XRF, XPS, H_2-TPR, BET, TEM, and TGA. Ni,Pd,Pt/$Mg_{0.85}Zr_{0.15}O$ catalyst exhibited the highest activity resulting in favorable CO_2 and CH_4 conversion rates of 99 % and 91 %, respectively, and suitable H_2/CO ratio 1.28 at temprature 900 °C and 1:1 of CH_4:CO_2 ratio. The different results of the catalysts showed that the catalytic performances of the catalysts strongly depended on the nature and concentration of promoter. The stability of Ni,Pd,Pt/$Mg_{0.85}Zr_{0.15}O$ catalyst was investigated for 200 h, and in the presence of 1.25 % stream of oxygen the stability was increased, resulting in a decrease in the coke deposition and a high conversion of CH_4 which increased from 91 to 96 %.

Acknowledgement

The researcher are grateful to NanoMite Grant (Vot. No: 5526308) for the provision of the necessary funds for conducting this research study. I expresses heartfelt thanks to Prof. Taufiq Yap Yun-Hin for his help and introduce all facilities.

References

[1] Sutthiumporn, K., Maneerung, T., Kawi, S. (2012). CO_2 Dry-reforming of Methane over $La_{0.8}Sr_{0.2}Ni_{0.8}M_{0.2}O_3$ Perovskite (M= Bi, Co, Cr, Cu, Fe): Roles of Lattice Oxygen on C-H Activation and Carbon Suppression. *International J. Hydrogen Energy*, 37: 11195-11207.

[2] Rahimpour, M.R., Aboosadi, Z.A., Jahanmiri, A.H. (2011). Optimization of Tri-reformer Reactor to Produce Synthesis Gas for Methanol Production using Differential Evolution (DE) Method. *Applied Energy*, 88: 2691-2701.

[3] Nur Nabilah, M.A., Dai-Viet, N., Azizan, M.T., Sumaia, Z.A. (2016). Carbon Dioxide Dry Reforming of Glycerol for Hydrogen Production using Ni/ZrO_2 and Ni/CaO as Catalysts. *Bulletin of Chemical Reaction Engineering & Catalysis*. 11(2); 200-209.

[4] Sarkari, M., Fazlollahi, F., Ajamein, H., Atashi, H., Hecker, W.C., Baxter, L.L. (2014). Catalytic Performance of an Iron-based Catalyst in Fischer–Tropsch Synthesis. *Fuel Process Technology*, 127: 163-170.

[5] Ayodele, B.V., Khan, M.R., Cheng, C.K. (2016). Production of CO-rich Hydrogen Gas from Methane Dry Reforming over Co/CeO_2 Catalyst. *Bulletin of Chemical Reaction Engineering & Catalysis*, 11(2): 210-219.

[6] Gangadharan, P., Kanchi, K.C., and Lou, H.H. (2012). Evaluation of the Economic and Environmental Impact of Combining Dry Reforming with Steam Reforming of Methane. *Chemical Engineering Research and Design*, 90(11): 1956-1968.

[7] Kehres, J., Jakobsen, J.G., Andreasen, J.W., Wagner, J.B., Liu, H., Molenbroek, A., Vegge, T. (2012). Dynamical Properties of a Ru/$MgAl_2O_4$ Catalyst During Reduction and Dry Methane Reforming. *J. Physical Chemistry, C*, 116: 21407-21415.

[8] Garcia-Dieguez, M., Pieta, I.S., Herrera, M.C., Larrubia, M.A., Alemany, L.J. (2011). Rh-Ni Nanocatalysts for the CO_2 and CO_2+H_2O Reforming of Methane. *Catalysis Today*, 172: 136-142.

[9] Menegazzo, F., Signoretto, M., Canton, P., Pernicone, N. (2012). Optimization of Bimetallic Dry Reforming Catalysts by Tem-

perature Programmed Reaction. *Applied Catalysis A*, 439: 80-87.

[10] Al-Doghachi, F.A., Rashid, U., Taufiq-Yap, Y.H. (2016). Investigation of Ce (III) Promoter Effects on the Tri-metallic Pt,Pd,Ni/MgO Catalyst in Dry-reforming of Methane. *RSC Advances*, 6(13): 10372-10384.

[11] Yu, M., Zhu, K., Liu, Z., Xiao, H., Zhou, X. (2014). Carbon Dioxide Reforming of Methane over Promoted $Ni_xMg_{1x}O$ (111) Platelet Catalyst Derived from Solvothermal Synthesis. *Applied Catalysis B Environment*, 148: 177-190.

[12] Al-Doghachi, F.A., Rashid, U., Zainal, Z., Saiman, M.I., Yap, Y.H.T. (2015). Influence of Ce_2O_3 and CeO_2 Promoters on Pd/MgO Catalysts in the Dry-reforming of Methane. *RSC Advances*, 5(99): 81739-81752.

[13] Aldbea, F., Ibrahim, N., Abdullah, M., Shaiboub, R. (2012). Structural and Magnetic Properties of $TbxY_{3-x}Fe_5O_{12}$ ($0 \leq x \leq 0.8$) Thin Film Prepared via Sol-Gel Method. *J Sol-gel Science Technology*, 62: 483-489.

[14] Grange, P. (1980). Catalytic Hydrodesulfurization. *Catalysis Review Science Engineer,* 21: 135-181.

[15] Abimanyu, H., Kim, C.S., Ahn, B.S., Yoo, K.S. (2007). Synthesis of Dimethyl Carbonate by Transesterification with Various MgO-CeO_2 Mixed Oxide Catalysts. *Catalysis Letter*, 118: 30-35.

[16] Chen, X., Jiang, J., Tian, S., Li, K. (2015). Biogas Dry Reforming for Syngas Production: Catalytic Performance of Nickel Supported on Waste-derived SiO_2. *Catalysis Science Technology*, 5: 860-868.

[17] Zhiijian, M., Ying, L., Maohong, F., Ling, Z. (2015). *J. Chemical Engineering*, 259: 293.

[18] Hidalgo, C., Jalila, S., Alberto, M., Said, S. (2012). XPS Evidence for Structure–Performance Relationship in Selective Hydrogenation of Crotonaldehyde to Crotyl Alcohol on Platinum Systems Supported on Natural Phosphates. *J. Colloid Interface Science*, 382: 67-73.

[19] Mahoney, E.G., Pusel, J., Stagg-Williams, S., Faraji, S. (2014). The Effects of Pt Addition to Supported Ni Catalysts on Dry (CO_2) Reforming of Methane to Syngas. *J. CO_2 Utilization*, 6: 40-44.

[20] Bao, Z., Lu, Y., Han, J., Li, Y., Yu, F. (2015). Highly Active and Stable Ni-based Bimodal Pore Catalyst for Dry Reforming of Methane. *Applied Catalysis A: General*, 491: 116-126.

[21] Rotaru, C.G., Postole, G., Florea, M., Matei-Rutkovska, F., Pârvulescu, V.I. (2015). Dry Reforming of Methane on Ceria Prepared by Modified Precipitation Route. P Gelin. *Applied Catalysis A: General,* 494: 29-40.

[22] Tada, S., Shimizu, T., Kameyama, H., Haneda, T. (2012). Ni/CeO_2 Catalysts with High CO_2 Methanation Activity and High CH_4 Selectivity at Low Temperatures. *International J. Hydrogen Energy*, 37: 5527-5531.

[23] Gonzalez-Delacruz, V.M., Ternero, F., Peren, R., Caballero, A., Holgado, J.P. (2010). Study of Nanostructured Ni/CeO_2 Catalysts Prepared by Combustion Synthesis in Dry Reforming of Methane. *Applied Catalysis A: General*, 384: 1-9.

[24] Koo, K.Y., Roh, H.S., Seo, Y.T., Seo, D.J., Yoon, W.L., Park, S.B. (2008). A Highly Effective and Stable Nano-sized Ni/MgO-Al_2O_3 Catalyst for Gas to Liquids (GTL) Process. *International J. Hydrogen Energy*, 33: 2036.

[25] Mei, Z., Li, Y., Fan, M., Zhao, L., Zhao, J. (2015). Effect of The Interactions between Pt Species and Ceria on Pt/Ceria Catalysts for Water Gas Shift: The XPS Studies. *Chemical Engineering J.*, 259: 293-302.

[26] Djaidja, A., Libs, S., Kiennemann, A., Barama, A. (2006). Characterization and Activity in Dry Reforming of Methane on NiMg/Al and Ni/MgO Catalysts. *Catalysis Today*, 113: 194-200.

[27] Kim, H.W., Kang, K.M., Kwak, H. (2009). Recent Developments and Achievements in Partial Oxidation of Methane With and Without Addition of Steam. *International J. Hydrogen Energy*, 34: 3351.

[28] Ahmed, W., Awadallah, A.E., Aboul-Enein, A.A. (2016). Ni/CeO_2-Al_2O_3 Catalysts for Methane Thermo-catalytic Decomposition to COx-free H_2 Production, *International Journal of Hydrogen Energy*, 41(41): 18484-18493.

[29] Mojović, Z., Mentus, S, Tesic, Z. (2004). Introduction of Pt and Pd Nanoclusters in Zeolite Cavities by Thermal Degradation of Acetylacetonates. *Material Science Forum*, 453: 257-262.

[30] Al-Doghachi, F.A., Islam, A., Zainal, Z., Saiman, M.I., Embong, Z., Taufiq-Yap, Y.H. (2016). High Coke-Resistance Pt/$Mg_{1-x}Ni_xO$ Catalyst for Dry Reforming of Methane. *PloS One*, 11(1): e0145862.

[31] Zecchina, A., Spoto, G., Coluccia, S., Guglielminotti, E. (1984). Spectroscopic Study of the Adsorption of Carbon Monoxide on Solutions of Nickel Oxide and Magnesium Oxide. Part 2. Samples Pretreated with Hydrogen. *Journal of the Chemical Society. Faraday Trans*, 80: 1891-1901.

[32] Hu, Y.H., Ruckenstein, E. (2003). Multiple Transient Response Methods to Identify

Mechanisms of Heterogeneous Catalytic Reactions. *Acco. Chem. Res.*, 36: 791-797.

[33] Appari S, Janardhanan VM, Bauri R, Jayanti S, Deutschmann O (2014) A Detailed Kinetic Model for Biogas Steam Reforming on Ni and Catalyst Deactivation due to Sulfur Poisoning. *Applied Catalysis A: General*, 471: 118-125.

[34] Djinović, P., Osojnik, G., Erjavec, B., Pintar, A. (2012). Influence of Active Metal Loading and Oxygen Mobility on Coke-free Dry Reforming of Ni-Co Bimetallic Catalysts. *Applied Catalysis B: Environment,* 125: 259-270.

[35] Topalidis, A., Petrakis, D.E., Ladavos, A., Loakatzikou, L., Pomonis, P.J. (2007). A Kinetic Study of Methane and Carbon Dioxide Interconversion over 0.5% Pt/$SrTiO_3$ Catalysts. *Catalysis Today*, 127: 238-245.

[36] Nakagawa, K., Kikuchi, M., Nishitani-Gamo, M., Oda, H., Gamo, H., Ogawa, K., Ando, T. (2008). CO_2 Reforming of CH_4 over Co/oxidized Diamond Catalyst, *Energy & Fuels,* 22(6): 3566-3570.

[37] Osaki, T., Mori, T. (2001). Role of Potassium in Carbon-free CO_2 Reforming of Methane on K-promoted Ni/Al_2O_3 Catalysts. *J. Catalysis*, 204: 89-97.

[38] Al-Fatesh, A.S., Naeem, M.A., Fakeeha, A.H., Abasaeed, A.E. (2013). CO_2 Reforming of Methane to Produce Syngas over γ-Al_2O_3-Supported Ni-Sr Catalysts, *Bulletin of the Chemical Society of Japan*, 86(6): 742-748.

[39] Giordano, F., Trovarelli, A., Leitenburg, C., Giona, M. (2000). A Model for the Temperature-Programmed Reduction of Low and High Surface Area Ceria. *Catalysis*, 193: 273-282.

[40] Steinhauer, B., Kasireddy, M., Radnik, J., Martin, A. (2009). Development of Ni-Pd Bimetallic Catalysts for the Utilization of Carbon Dioxide and Methane by Dry Reforming. *Applied Catalysis A: General*, 366: 333-341.

[41] Istadi, I., Anggoro, D.D., Amin, N.A.S., Ling, D.H.W. (2011). Catalyst deactivation simulation through carbon deposition in carbon dioxide reforming over Ni/CaO-Al_2O_3 catalyst. *Bulletin of Chemical Reaction Engineering & Catalysis*, 6(2): 129-136.

[42] Miguel, S., Vilella, I., Maina, S., Jose-Alonso, D., Roman-Martinez, M., Illan-Gomez, M. (2012). Influence of Pt Addition to Ni Catalysts on the Catalytic Performance for Long Term Dry Reforming of Methane. *Applied Catalysis A: General*, 435: 10-18.

[43] Zhang, H., Li, M., Xiao, P., Liu, D., Zou, C.J. (2013). Structure and Catalytic Performance of Mg-SBA-15-Supported Nickel Catalysts for CO_2 Reforming of Methane to Syngas, *Chemical Engineering & Technology*, 36(10): 1701-1707.